Mineralium Deposita (2019) 54:507–524
https://doi.org/10.1007/s00126-018-0821-5

ARTICLE

Textural characteristics and trace element distribution in carbonate-hosted Zn-Pb-Ag ores at the Paleoproterozoic Black Angel deposit, central West Greenland

S. Horn[1] · A. Dziggel[1] · J. Kolb[2,3] · S. Sindern[1]

Received: 19 December 2017 / Accepted: 26 June 2018 / Published online: 12 July 2018

Abstract

The Black Angel deposit represents the most important base metal deposit in Greenland, having produced 11.2 million tons of Pb-Zn-Ag ore from 1973 to 1990. The deposit is hosted by a greenschist facies calcitic marble of the Mârmorilik Formation of the Paleoproterozoic Karrat Group. The ore consists of sphalerite, pyrite, and galena, with minor amounts of chalcopyrite, arsenopyrite, tetrahedrite, freibergite, tennantite, stannite, briartite, rutile, and graphite. Pyrite occurs as porphyroclasts and as fine-grained euhedral grains and is commonly surrounded by sphalerite, galena, and chalcopyrite. Deformation textures such as pyrite annealing, fracture healing by sulfides as well as "Durchbewegung" textures are common. Electron microprobe analysis and laser ablation-inductively coupled plasma-mass spectrometry trace element analysis show that tetrahedrite-freibergite and galena are enriched in Ag and represent the main Ag carriers. Galena also hosts substantial amounts of Sb, Sn, and Bi. The presence of Ge-rich chalcopyrite and briartite ($Cu_2(Zn,Fe)GeS_4$) inclusions in sphalerite indicates that the Black Angel deposit may be host to an hitherto unrecognized Ge endowment. It is suggested that sphalerite and briartite co-precipitated from a hydrothermal fluid having an intermediate sulfidation state. The origin of the deposit remains ambiguous. The calcitic host rock, epigenetic style of mineralization, presence of anhydrite, and occurrence of hydrothermal breccias are consistent with an origin as Mississippi Valley-type deposit. However, much of the mineralization is syn- to late-tectonic and syn-metamorphic, and the sulfide textures are consistent with a metamorphic overprint. An origin as carbonate-hosted polymetallic Kipushi-type deposit is thus more likely, since these deposits constitute the primary deposit type from which briartite has been previously documented.

Keywords Black Angel deposit · Carbonate-hosted Zn-Pb-Ag deposit · Trace element composition of sulfides · Briartite · Greenland

Editorial handling: T. Monecke

Electronic supplementary material The online version of this article (https://doi.org/10.1007/s00126-018-0821-5) contains supplementary material, which is available to authorized users.

✉ S. Horn
stefan.horn@rwth-aachen.de

[1] Institute of Applied Mineralogy and Economic Geology, RWTH Aachen University, Wüllnerstrasse 2, 52062 Aachen, Germany

[2] Department of Petrology and Economic Geology, Geological Survey of Denmark and Greenland, Øster Voldgade 10, 1350 Copenhagen K, Denmark

[3] Present address: Institute of Applied Geosciences, Karlsruhe Institute of Technology, Adenauerring 20b, 76131 Karlsruhe, Germany

Introduction

The Black Angel deposit is a world class Zn-Pb-Ag deposit (Kolb et al. 2016; Rosa et al. 2016, 2017) located in central West Greenland, approximately 500 km north of the Arctic Circle. The deposit was in production between 1973 and 1990 during which 11.2 million tons of ore grading 12.3% Zn, 4.0% Pb, and 29 ppm Ag were extracted (Thomassen 2006). A total of ten ore bodies were exploited, including two satellite ore bodies at ~ 3 km distance to the main deposit.

Despite the long mining history and recent exploration work, the processes that resulted in the formation of the carbonate-hosted Zn-Pb-Ag deposit are not well understood (Thomassen 2006). The deposit has been classified as a syngenetic sediment-hosted massive sulfide deposit (SHMS) or an epigenetic Mississippi Valley type (MVT)

deposit. The wall rocks are deformed and metamorphosed to greenschist facies conditions, and early studies suggest that at least some of the ore was remobilized after deposition (Pedersen 1980, 1981).

To provide new insight into the processes and conditions of ore formation and to study the potential trace element content of the sulfide minerals, this study investigates the petrography and mineral chemistry of ore samples from the different ore zones, using electron microprobe analyses (EMPA) and laser ablation-inductively coupled-plasma mass spectrometry (LA-ICP-MS). The composition of the ore minerals was also studied to determine the mineralogical sequestration of Ag, which represented an important by-product of the mine.

Geological setting

The Black Angel deposit is situated in the Rinkian Orogen in central West Greenland, at around 71°N, 51°E, and 600 m above sea level (Fig. 1). The Rinkian Orogen has been interpreted to represent the northern continuation of the Nagssugtoqidian Orogen, which formed during the Paleoproterozoic collision of the North Atlantic Craton in the S and the Rae Craton in the N (Grocott and Pulvertaft 1990; van Gool et al. 2002; Thrane et al. 2005; Connelly et al. 2006). However, recent studies document a more complex evolution and the presence of an earlier SE-vergent thrust system, which is inconsistent with a N-S directed convergence of the Nagssugtoqidian Orogen (Grocott and McCaffrey 2017).

The Rinkian Orogen is made up of metasedimentary and metavolcanic rocks of the Paleoproterozoic Karrat Group, which unconformably overlies an Archean basement dominated by orthogneiss (Fig. 1b). The Karrat Group is subdivided into four formations, including the Qeqertarssuaq, Mârmorilik, Kangilleq, and Nûkavsak formations (Fig. 1b; Henderson and Pulvertaft 1967; Rosa et al. 2016, 2017; Grocott and McCaffrey 2017). The Qeqertarssuaq and Mârmorilik formations are considered as lateral equivalents, whereas the Kangilleq and Nûkavsak formations structurally overlie the Qeqertarssuaq Formation (Rosa et al. 2016). Uranium-Pb dating of detrital zircons reveals a maximum deposition age for the Nûkavsak Formation of 1953 ± 31 Ma (Sanborn-Barrie et al. 2017). A Pb-isotope whole rock

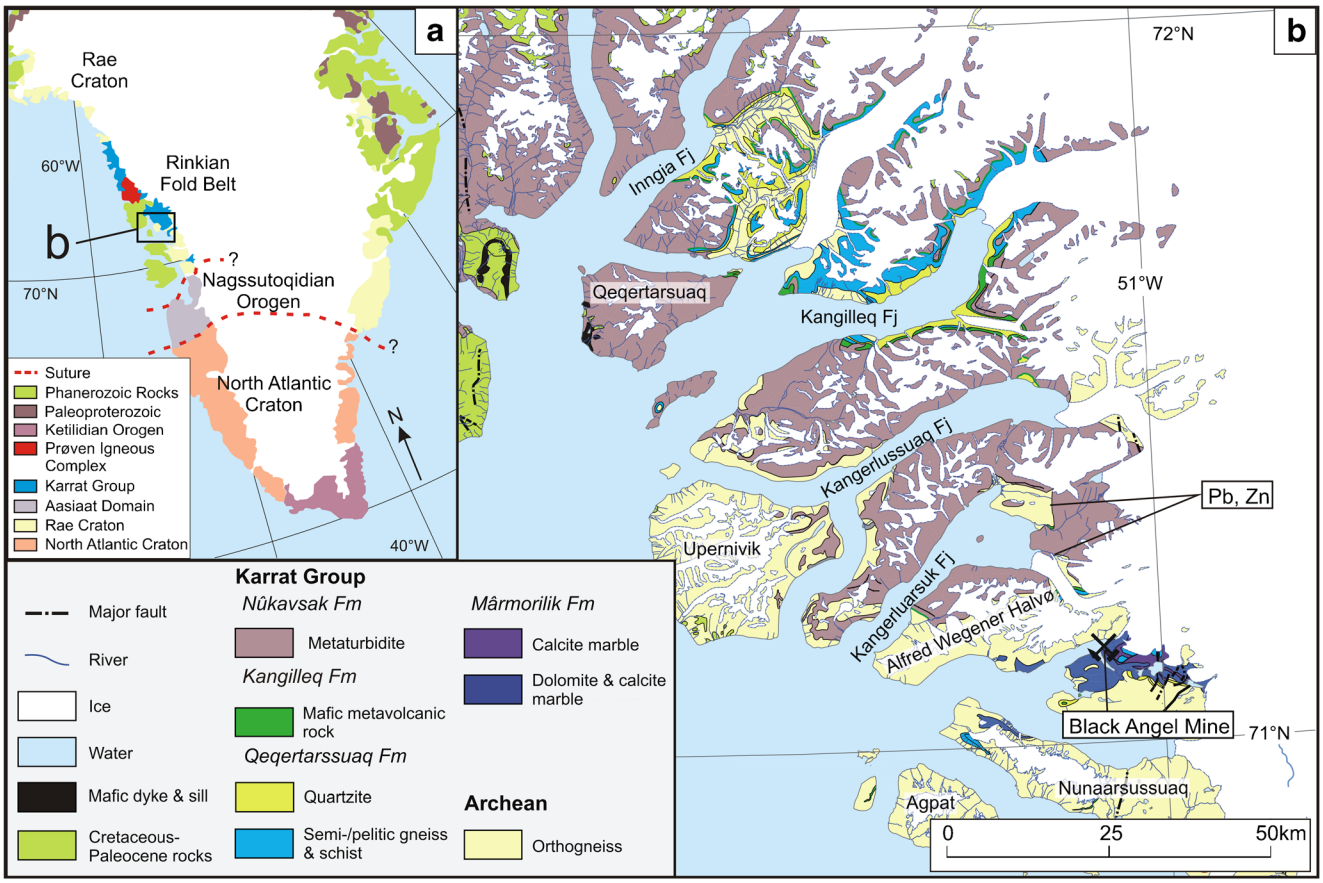

Fig. 1 **a** Geological map of Greenland. The Rae Craton is depicted in the north, while the North Atlantic Craton is situated in the south (modified after St-Onge et al. 2009). **b** Regional lithological map of the area around the Black Angel deposit, showing the distribution of the lithologies of the Karrat Group and underlying Archean basement. Metaturbidites of the Nûkavsak formation have the largest regional extent (modified after Rosa et al. 2016)

isochron from the ore-hosting marbles of the Mârmorilik Formation yields an age of 1881 ± 20 Ma, which is interpreted as the age of metamorphic recrystallization (Taylor and Kalsbeek 1990).

The Black Angel deposit is hosted by the carbonate-dominated Mârmorilik Formation, which is exposed between Nunnarssusuaq in the S and the Alfred Wegener Halvø in the N (Fig. 1b). The lowest unit of the Mârmorilik Formation consists of mainly quartzite and metasemipelite in the lower part and dolomite marble in the upper part (Garde 1978). The middle Mârmorilik Formation consists of an interbedded calcite-dolomite marble, while the upper Mârmorilik Formation is composed of calcitic marble. Metasemipelitic layers of various thicknesses are present. The Mârmorilik Formation deposited in a sub-basin during subsidence of the Karrat basin, having a maximum thickness of 2 km (Garde 1978).

The Maarmorilik area is characterized by normal faults trending N-S to NE-SW, which were recognized on Nunaarsussuaq and in the South Lakes region. In addition, folds with NW-SE- to WNW-ESE-oriented fold axes and SSE to SE-directed thrusts are present (Garde 1978; Rosa et al. 2016, 2017). These structures formed during three stages of deformation. The normal faults are of syn-sedimentary origin and likely formed during E-W to NW-SE extension (Garde 1978; Rosa et al. 2016). Subsequently, these extensional faults were inverted during SE-directed thrusting (Grocott and McCaffrey 2017). The last stage of deformation was associated with the development of NNW-vergent thrusts, which overprint the earlier structures (Rosa et al. 2016). This stage was probably related to ongoing crustal shortening in the Nagssugtoqidian Orogen along its northern margin (Grocott and McCaffrey 2017).

Rocks of the Mârmorilik Formation experienced greenschist facies metamorphism (Garde 1978). Temperature estimates from calc-silicate mineral assemblages infer that peak temperatures did not exceed 500 °C (Pedersen 1980).

Orebodies and textures

The orebodies in the Mârmorilik Formation are subhorizontal, massive to semi-massive, and stratabound sheets that mainly occur within the calcitic marble. Nine orebodies have been documented at Black Angel Mountain spanning over a 3 km long and 600 m wide zone (Fig. 2a–c; Pedersen 1980; Thomassen 2006). Two additional orebodies are found on the Maarmorilik Plateau and are referred to as the Nuungarut Zones 1 and 2 (Fig. 2d; Thomassen 2006). The orebodies reach a thickness of up to 35 m (Pedersen 1980). The major ore minerals are sphalerite, pyrite, galena, and chalcopyrite. Minor phases include arsenopyrite, pyrrhotite, stannite, löllingite, enargite, bornite, polybasite, rutile, hematite, magnetite, electrum, and graphite (Pedersen 1980).

The Angel Zone and the Cover Zone are the largest orebodies, containing 78.5% of the total ore. They are bound by N-S trending fault zones (Pedersen 1980). The Angel Zone is located in the northwestern part of Black Angel Mountain (Figs. 2c and 3). In a study on the Angel Zone, Pedersen (1980, 1981) documented several stages of mineralization that were interpreted to have formed in response to mobilization during metamorphism. Figure 3 shows an illustration of the Angel Zone with its three structural domains in relation to the ore types (Pedersen 1980). The lower part of the Angel Zone orebody consists of banded ore, characterized by millimeter to centimeter-thick layers of pyrite and sphalerite + galena, parallel to bedding in the adjacent marble (Pedersen 1980, 1981). The massive ore occurs in close gradational relationship to the banded ore with medium- to fine-grained sulfides, primarily sphalerite and galena. The porphyroclastic ore occurs in the southern structural domain and is characterized by medium- to coarse-grained pyrite surrounded by fine-grained sulfide minerals (Fig. 3). Furthermore, the remobilized ore is particularly abundant in the northern structural domain and is enriched in galena, sphalerite, tennantite, and minor phases such as chalcopyrite, stannite, or arsenopyrite. Structures in the main orebodies are (1) isoclinal to tight, E-trending folds; (2) S-vergent thrust sheets that are subparallel to bedding and that crosscut these folds; and (3) N-vergent open to tight folds with fold axes trending 90–125°, which fold the thrust sheets (Pedersen 1980). The structures are interpreted to have formed during three deformation stages. N-S directed compressional deformation resulted in the development of the E-trending isoclinal folds (D_1BA). During this stage, the banded ore, interpreted as the syngenetic ore, was deformed, isoclinally folded and mobilized, leading to the emplacement of chalcopyrite, galena, and sphalerite into low-strain areas. Successively, S-directed thrusting resulted in the formation of distinct thrust planes (Fig. 3; D_2BA; Pedersen 1980, 1981). The higher strain likely caused the main mobilization during D_2BA, resulting in the formation of the porphyroclastic ore, which is closely associated with these thrust planes. Subsequently, N-vergent open to tight folds formed during D_3BA. These structures are the main host for the remobilized ore (Pedersen 1980).

Materials and methods

In total, 43 samples were investigated, which were primarily collected in 1989 by Mogens Lind for the reference collection at the Geological Survey of Denmark and Greenland (GEUS) in Copenhagen (Electronic Supplementary Material, ESM 1; Fig. 2). The sample set includes three large exhibition samples (E-1–E-3) of GEUS.

Following careful petrographic inspections, the major element compositions of pyrite, sphalerite, chalcopyrite,

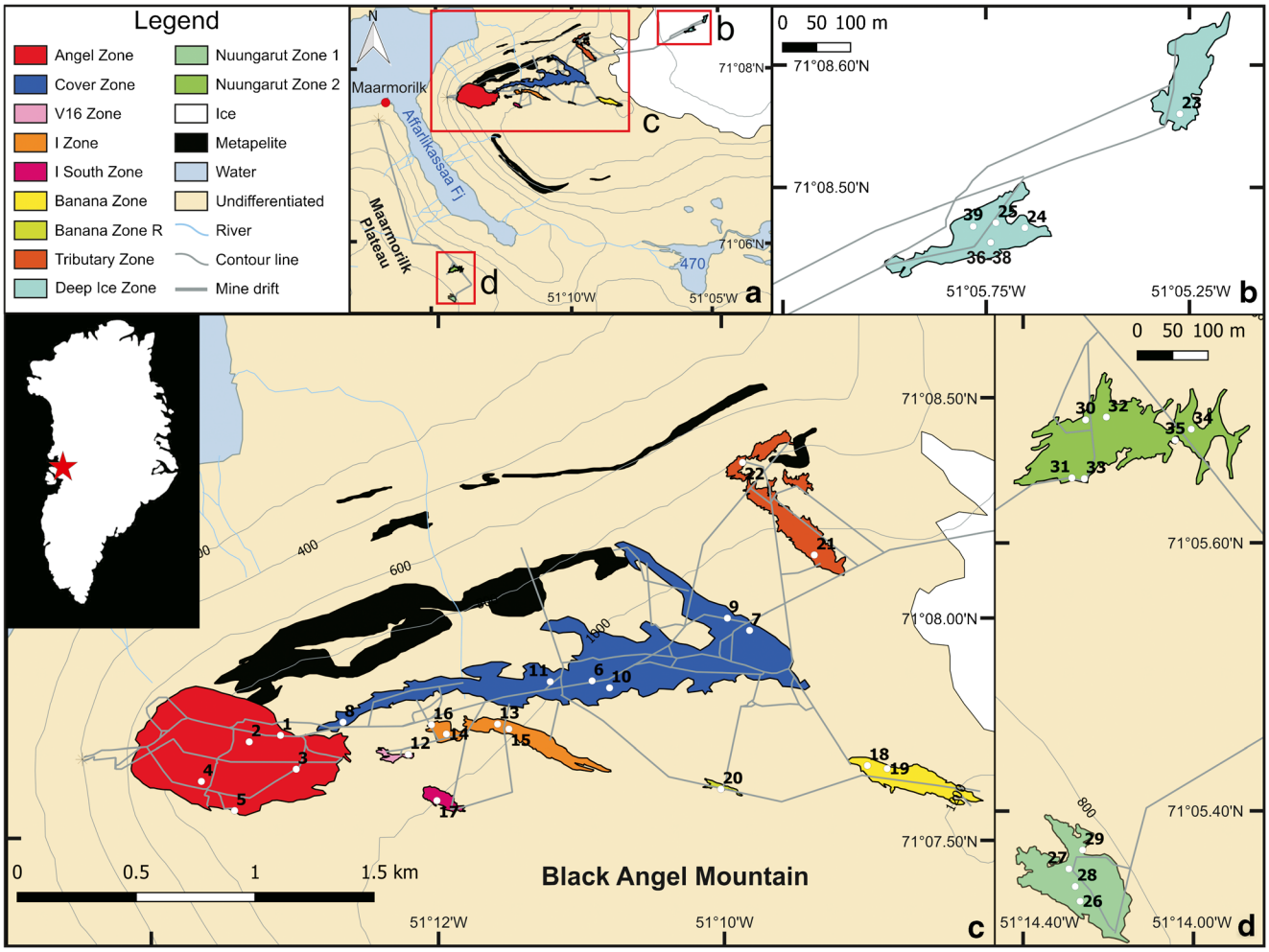

Fig. 2 The Black Angel deposit orebodies and sample locations (based on mine maps from Greenex A/S 1990). **a** Overview of the orebodies. **b** Deep Ice Zone. **c** Major orebodies of the Black Angel deposit. **d** Nuungarut Zone 1 and 2. The sample numbers correspond to the two last digits of sample numbers given in ESM 1

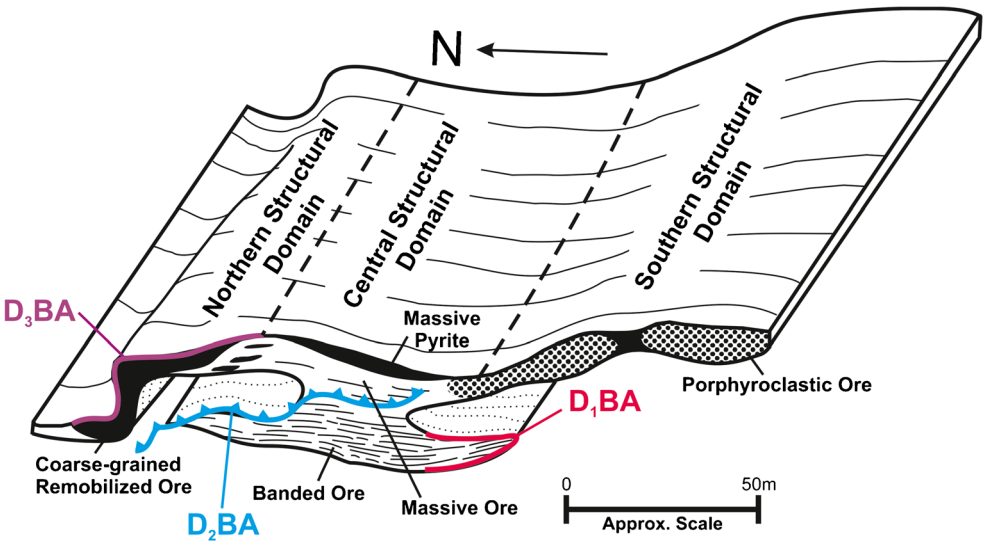

Fig. 3 Illustration of the Angel Zone orebody with structural domains and ore tectonites (modified after Pedersen 1980)

tetrahedrite-freibergite, stannite, and briartite were determined in polished sections of nine representative samples using a JEOL JXA 8900R electron microprobe at the Institute of Applied Mineralogy and Economic Geology (IML) at RWTH Aachen University. Samples were analyzed using an acceleration voltage of 25 kV, a beam current of 28 nA, and a focused beam with a diameter of ~ 1 μm. All samples were carbon-coated prior to analysis. Natural and synthetic standards were used for calibration. X-ray compositional maps for selected elements in pyrite were collected using wavelength-dispersive X-ray detectors on the same machine.

The trace element concentrations of the sulfide minerals were determined by LA-ICP-MS at the IML, using a NewWave UP193FX excimer laser with an ArF-gas mixture and a wavelength of 193 nm. The pulse rate of the laser was set to 4 Hz with an irradiation of ~ 0.78–0.94 GW/cm and a beam fluence of ~ 4.0–4.7 J/cm^2. The spot size varied between 100 and 150 μm. The ablation cell was purged by constant He-gas flow of 0.6 l/min. After the ablation, Ar-gas with a flow rate of 0.8 l/min was conducted to the He-gas. The gas mixture carried the aerosols into the inductively coupled plasma. The inductively coupled plasma is set to a radio frequency power of 1200 W. The plasma gas flow was constant at 15 l/min and the auxiliary gas flow was set to 1.2 l/min. A PerkinElmer Elan DRCe quadrupole mass spectrometer was used. Each measurement included determination of the background signal for 60 s, followed by 30 s of laser ablation. Twenty isotopes were monitored during the analysis: ^{34}S, ^{51}V, ^{55}Mn, ^{57}Fe, ^{59}Co, ^{60}Ni, ^{69}Ga, ^{70}Zn, ^{73}Ge, ^{75}As, ^{107}Ag, ^{111}Cd, ^{115}In, ^{118}Sn, ^{121}Sb, ^{197}Au, ^{202}Hg, ^{205}Tl, ^{208}Pb, and ^{209}Bi. Lead was not analyzed in galena due to the expected high peaks. Sulfur was used as an internal standard. Calibration was carried out using the synthetic polymetallic sulfide reference material MASS-1 from the US Geological Survey (Wilson et al. 2002). Analyses of the reference materials were run before and after every sixth sample analyses to correct for instrumental drift. The detection limit (DL) was calculated using the 6σ-criterion. Data reduction was conducted using the Microsoft Excel sheets by Hattendorf (2000). Intervals of signal integration were adjusted to avoid the influence of locally occurring micro-inclusions of Pb and Ag (see below), leading to variable signals (ESM 2a, b).

Petrography

The samples investigated in this study are mainly composed of sphalerite, pyrite, and galena, whereas chalcopyrite, arsenopyrite, various sulfosalts, and graphite occur as minor minerals in the orebodies (ESM 1). Following the classification into different ore tectonites (Pedersen 1980), most of the samples can be classified as porphyroclastic ore (ESM 1). Two samples show distinct layering, characteristic of the banded ore. One of these samples additionally contains massive monomineralic ore in contact with the banded ore (ESM 1).

Pyrite

Pyrite is medium- to coarse-grained and mainly forms euhedral to subhedral grains (Fig. 4a–d). Different generations have been observed. In some samples, pyrite contains inclusions of sphalerite, galena, chalcopyrite, and/or gangue minerals, which outline an older core (type 1 pyrite; Py-1) that is overgrown by a younger rim (type 2 pyrite; Py-2) (Fig. 4a). In other samples (Fig. 4b), type 1 pyrite is characterized by coarse and rounded anhedral grains, whereas type 2 pyrite is fine- to medium-grained and has a euhedral to subhedral shape. Pyrite in most samples shows different degrees of fracturing. In some samples, the contact between the intergrown pyrite grains is marked by a triple junction of 120° (Fig. 4a), indicative of pyrite annealing (Vokes and Craig 1993). Both pyrite annealing and overgrowth occur in the banded ore and the porphyroclastic ore (Pedersen 1980).

Sphalerite

Sphalerite is the major sulfide mineral and mainly forms the matrix around pyrite and gangue minerals (Fig. 4b, c). It is closely associated with galena and locally replaces type 1 pyrite along the rims (Fig. 4b). Sphalerite grains are predominantly anhedral and fine- to medium-grained. Locally, sphalerite occurs as rounded and typically small (2–50 μm) inclusions in types 1 and 2 pyrite (Fig. 4a, b), although some larger inclusions with a grain size of several hundred μm are locally present. Sphalerite is often enclosed by a galena matrix. This texture is known under the term "Durchbewegung" and is indicative of deformation (Vokes 1969; Gilligan and Marshall 1987). It mainly occurs in porphyroclastic ore and is related to D_2BA (Pedersen 1980). "Durchbewegung" can also be observed in the case of pyrite hosted in a sphalerite matrix, showing that sphalerite was less competent than pyrite (Fig. 4b). In some samples, sphalerite contains twin lamellae implying sphalerite deformation (Gilligan and Marshall 1987).

Galena

Galena commonly occurs in association with sphalerite, but is generally less abundant. The grains are fine-grained and

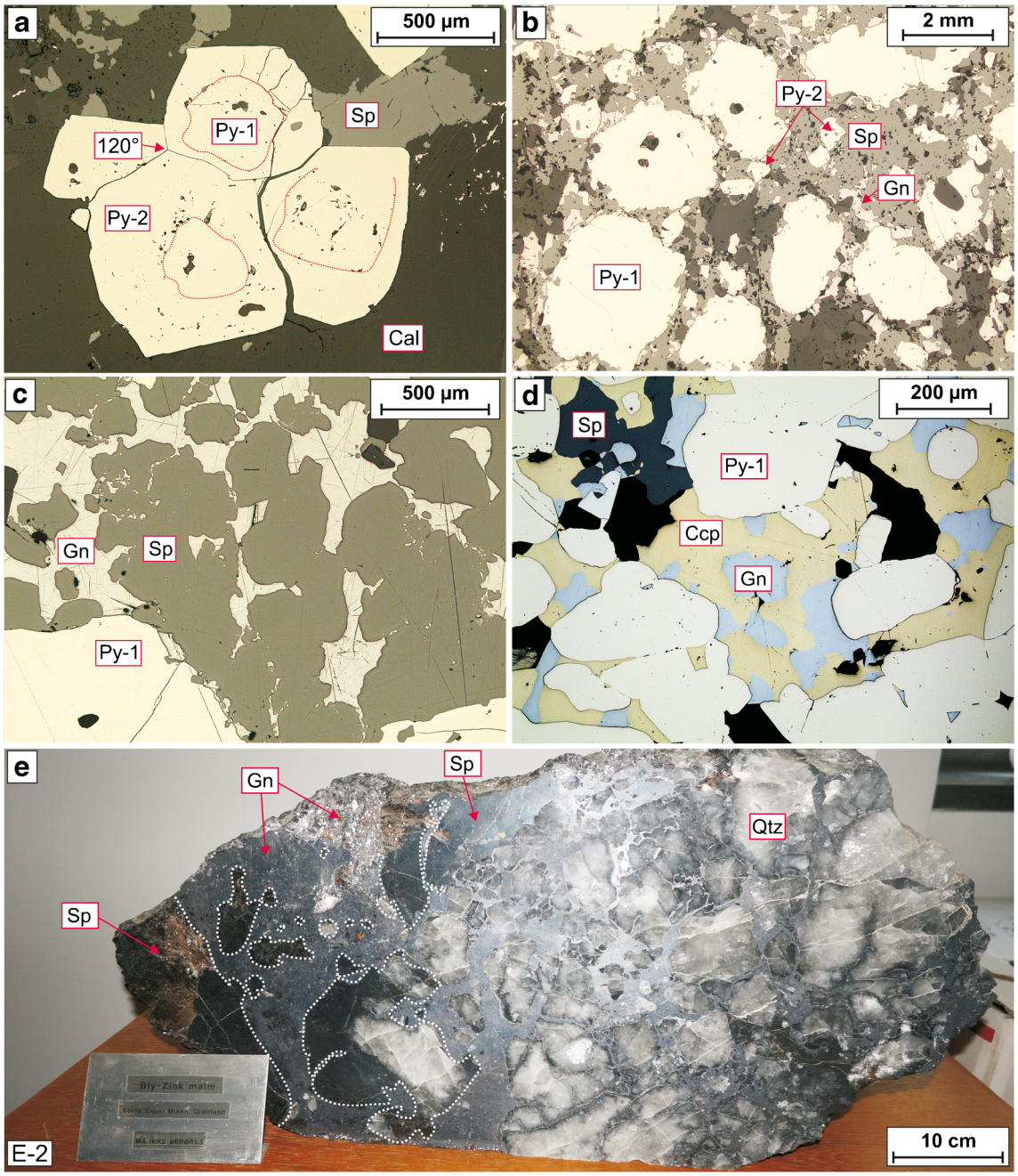

Fig. 4 Photomicrographs of the ore samples. **a** Inclusion patterns in pyrite (Py) defining two pyrite generations surrounded by calcite (Cal). The grains show annealing textures, as indicated by the 120° angle between the three grains (sample "V16", V16Z). Reflected light. **b** Two types of pyrite in a matrix dominated by sphalerite (Sp) and galena (Gn): Py-1 is coarse-grained, anhedral, and rounded, while Py-2 is euhedral to subhedral and fine- to medium-grained. Both pyrite types contain inclusions of sphalerite (Sp) and gangue-minerals (sample 367918 BZ). Reflected light. **c** Interstitial galena (Gn) between sphalerite grains. Sphalerite inclusions are present in type 1 pyrite, illustrated in the lower right corner (sample 367908, CZ). Reflected light. **d** Chalcopyrite (Ccp) associated with galena in a pyrite-rich layer of the banded ore. Pyrite is rounded (sample 367923, DIZ). Reflected light. **e** Brecciated ore made up of quartz (Qtz) and sphalerite that is invaded by galena vein. Quartz dominates the right side, while sphalerite is more abundant on the left. The white dashed lines outline sphalerite-quartz fragments. The abbreviations used for the different ore zones are given in ESM 1

anhedral and form an interstitial phase that locally replaces sphalerite (Fig. 4c). Galena can also be found along fractures in pyrite or along the rims of pyrite often in association with chalcopyrite (Fig. 4d). It fills the interstitial space between

calcite grains in one sample. Figure 4e shows a hydrothermal breccia with centimeter-scale galena veins crosscutting a former sphalerite-quartz ore. Galena-rich veins are also present in the pyrite-rich porphyroclastic ore.

Chalcopyrite

Chalcopyrite is mostly associated with galena, but is considerably less abundant and was not found in all samples (ESM 1). It predominantly occurs in association with type 1 pyrite (Fig. 4d), with grain sizes varying between 10 and 200 μm. Where present, chalcopyrite occurs along pyrite fractures or as an interstitial phase between fractured pyrite grains similar to galena. Chalcopyrite also occurs as small inclusions (20–50 μm) in sphalerite. This texture is known as "chalcopyrite disease", which many studies interpret as a replacement texture (Barton and Bethke 1987; Sugaki et al. 1987; Bente and Doering 1993, 1995). The chalcopyrite inclusions occur disseminated or along rims and lamellae of sphalerite.

Stannite group minerals

Two of the samples investigated contain the stannite group minerals stannite and briartite (Fig. 5a, b). The two minerals appear as small roundish to elongate inclusions in sphalerite, with a grain size of 30–250 μm. Briartite occurs in a sample of the banded ore within sphalerite layers. Locally, briartite contains inclusions of finely disseminated chalcopyrite and tennantite (Fig. 5a). Stannite occurs as small elongate anhedral grains in sphalerite in a sample of the porphyroclastic ore (Fig. 5b).

Tetrahedrite-freibergite and arsenopyrite

In a few samples, minerals of the tetrahedrite-freibergite series and arsenopyrite are found in association with galena (Fig. 5c). Tetrahedrite and freibergite occur as anhedral grains with a grain size of 20–100 μm. They are often surrounded by galena and sphalerite. Arsenopyrite is euhedral and forms small rhombohedral grains (20–100 μm), which are often fractured. Arsenopyrite was only recognized in two samples, where it occurs as inclusions in galena.

Rutile and graphite

Rutile was found in three samples and is typically anhedral with a grain size of 10–50 μm. It occurs in association with pyrite and sphalerite. In one sample, it occurs in a fracture in pyrite filled with galena.

Graphite is mostly very fine-grained and mainly associated with galena and, more rarely, sphalerite and pyrite (Fig. 5d). Locally, it forms thin rims around euhedral quartz grains.

Host rock fragments and gangue minerals

Calcitic and dolomitic marble as well as metapelite are present as up to several centimeter-large, rounded host rock fragments in several ore samples. They often contain disseminated pyrite and minor sphalerite and galena. The metapelite consists mainly of biotite, muscovite, and quartz. Massive fine-grained anhydrite was identified in the country rock (ESM 1).

Gangue minerals are mainly calcite and quartz. Calcite is fine-grained and associated with sphalerite and galena. Figure 5e shows the contact between dolomite, hydrothermal calcite, and sulfide minerals. Quartz is fine- to coarse-grained and often euhedral. Coarser aggregates of quartz are locally brecciated, and galena and type 2 pyrite occupy the fractures (Figs. 4e and 5f). Figure 5f displays a quartz grain containing fine calcite veins associated with galena. Quartz is often accompanied by graphite. Other gangue minerals that have been identified in the ore samples include hydrothermal fluorite and barite. Apatite and zircon locally occur as inclusions in pyrite and quartz.

Mineral chemistry

Pyrite

Pyrite was analyzed in six samples (ESMs 3, 4, 5). The grains are typically unzoned, and in most cases, the different types of pyrite do not record any marked compositional difference in minor or trace elements. The Fe concentration ranges from 45.9 to 47.0 wt.%, except for two analyses of type 2 pyrite, which have lower Fe (44.6 and 45.1 wt.%) and higher Zn concentrations (2.7 and 2.1 wt.%) (ESM 3). However, a general correlation between Fe and Zn is absent.

Arsenic is the most abundant trace element with an average concentration of 181 ppm (ESM 4). In two samples, high As values of up to 1770 ppm were found in the cores of two type 1 pyrite grains (ESM 5). X-ray mapping reveals that the high As concentrations either occur in small inclusion of As-enriched pyrite or in thin, As-rich growth bands (Fig. 6a–d). The concentration of other trace elements in pyrite is generally low (ESM 4). The Co concentration varies between the detection limit and 110 ppm, with an average of 19 ppm. Nickel occurs in similar but slightly lower concentration, with an average of 13 ppm.

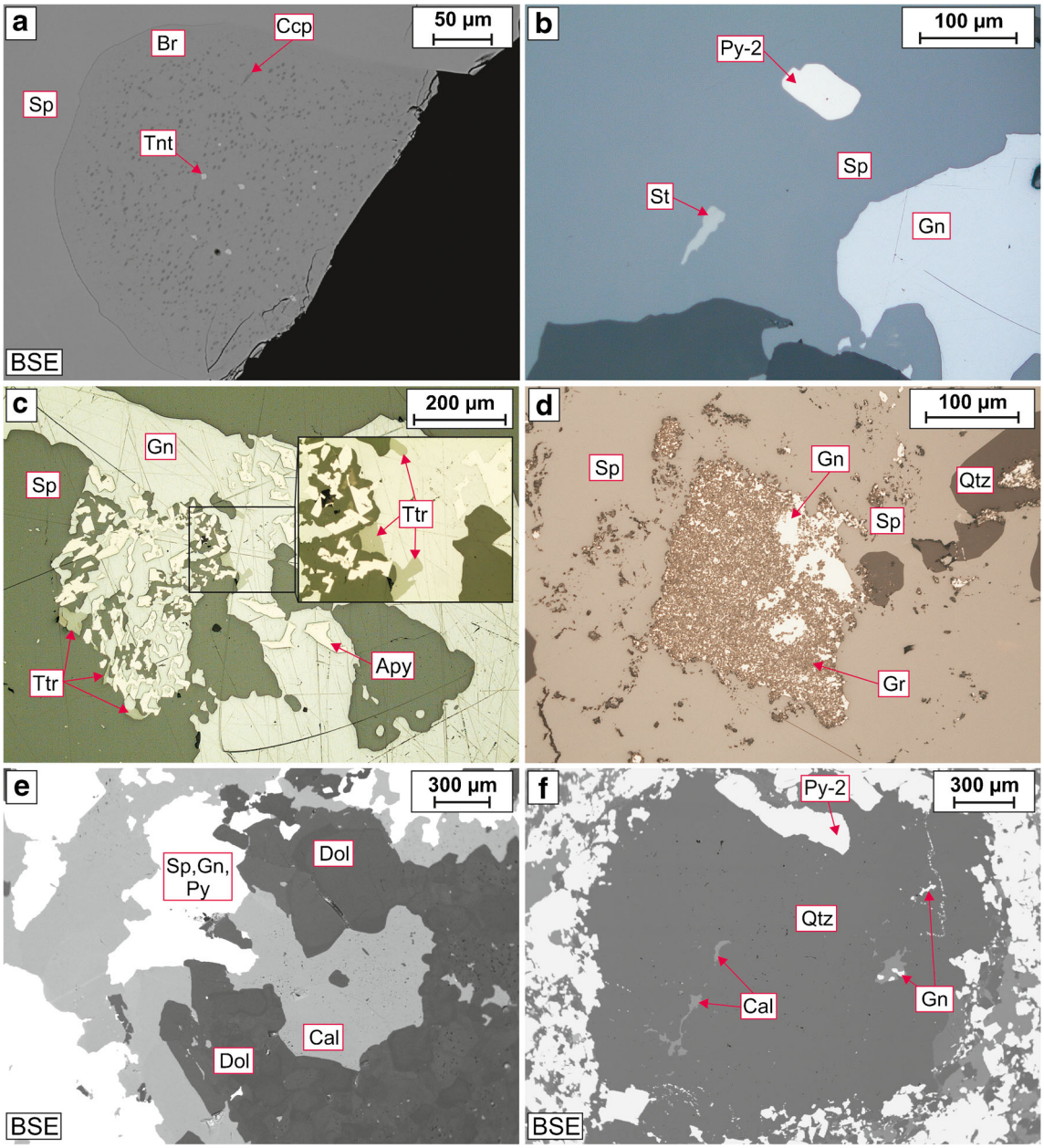

Fig. 5 Photomicrographs of ore samples. **a** Backscattered electron (BSE) image of a coarse briartite (Br) grain with inclusions of tennantite (Tnt) and chalcopyrite (Ccp) (sample 367923, DIZ). **b** Anhedral elongate inclusion of stannite (St) in sphalerite (sample 367921, TZ). Reflected light. **c** Tetrahedrite (Ttr) and arsenopyrite (Apy) inclusions in galena (Gn) in contact with sphalerite. Arsenopyrite is euhedral and partly fractured, while tetrahedrite appears anhedral and occurs in contact with sphalerite (Sp) (sample 367908, CZ). Reflected light. **d** Association of galena and graphite (Gr) surrounded by sphalerite (sample 367912; V16Z). Reflected light. **e** Calcite (Cal) and dolomite (Dol) in a massive ore. Dolomite is partly euhedral as can be seen in the lower left part of the image (sample 367921, TZ; BSE). **f** A rounded quartz (Qtz) grain with fractures filled by calcite and galena (sample 367930; N2Z; BSE). The abbreviations used for the different ore zones are given in ESM 1

Sphalerite

Sphalerite was analyzed in six samples (ESMs 3, 4, 5). The Fe content co-varies with the Zn concentration, but no zonation is visible. A galena-rich sample with minor pyrite exhibits the lowest Fe content in sphalerite, with an average of 1.7 wt.%, while the Fe content in the other samples ranges between 2.3 and 6.0 wt.%. Sphalerite inclusions in pyrite and the outermost rims of sphalerite at the contact to pyrite record the highest Fe concentrations (Fig. 6c).

Trace elements in sphalerite include Cd, Mn, Ga, Hg, Ag, Ge, and Sb (Fig. 7a–e; ESMs 4, 5). The Cd concentration ranges from 4540 to 6140 ppm (Fig. 7a). The Mn concentration varies between 30 and 563 ppm (Fig. 7b), while Ga contents of up to 115 ppm are recorded (Fig. 7c). The Mn and Ga concentrations show a positive correlation except for one sample (Fig. 7b). The Hg concentrations cluster tightly and range from 23 to 65 ppm, with a mean concentration of 42 ppm (Fig. 7d).

The Ag concentration in sphalerite is generally low, ranging between 2 and 24 ppm (Fig. 7e). In most cases, the Ag signal was stable, which indicates incorporation of Ag into the sphalerite crystal structure. Nevertheless, some analyses show distinct Ag peaks in the time-resolved ablation signal, pointing to micro- or nano-scale inclusions of Ag-bearing sulfides, sulfosalts, or native silver (ESM 2b). The Ge concentration in sphalerite is generally below the detection limit, except for two samples, where elevated values of 2–65 and 2–3 ppm are recorded (ESMs 4, 5). However, four of the spot analyses show no constant ablation signal, pointing to the presence of Ge-phase inclusions. The Sb concentration is also low with values of up to 23 ppm, and Sb is not detected in every sample. The concentration of In is dominantly below 1 ppm (ESM 4).

Galena

The major element composition in galena was determined in four samples, while trace element analyses were performed on six samples (ESMs 3, 4, 5). Galena does not show a major deviation from its ideal stoichiometry. The most important trace elements include Sb, Ag, Sn, Bi, and Cd (Fig. 8a–e). One sample from the porphyroclastic ore has the highest Sb and Ag concentrations of up to 738 and 649 ppm, respectively (Fig. 8a, b). Tin and Bi also show the highest concentrations in this sample, with values of up to 88 and 57 ppm, respectively (Fig. 8c, d). A single spot analysis in a galena inclusion in pyrite yields distinctly lower Sb and Ag concentrations (Fig. 8a, b).

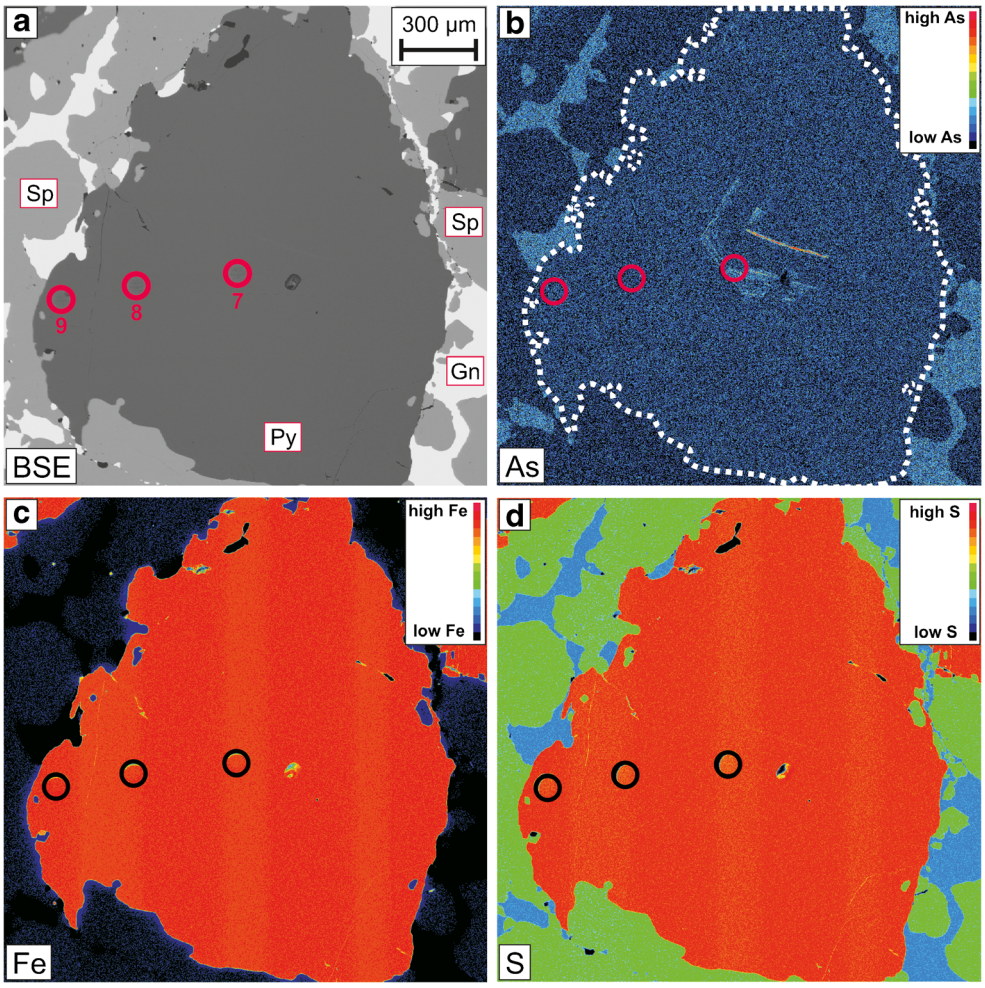

Fig. 6 **a** BSE image and **b**–**d** X-ray compositional maps of type 1 pyrite in sample 367908 (Cover Zone). The center of the grain contains growth bands with higher As concentrations

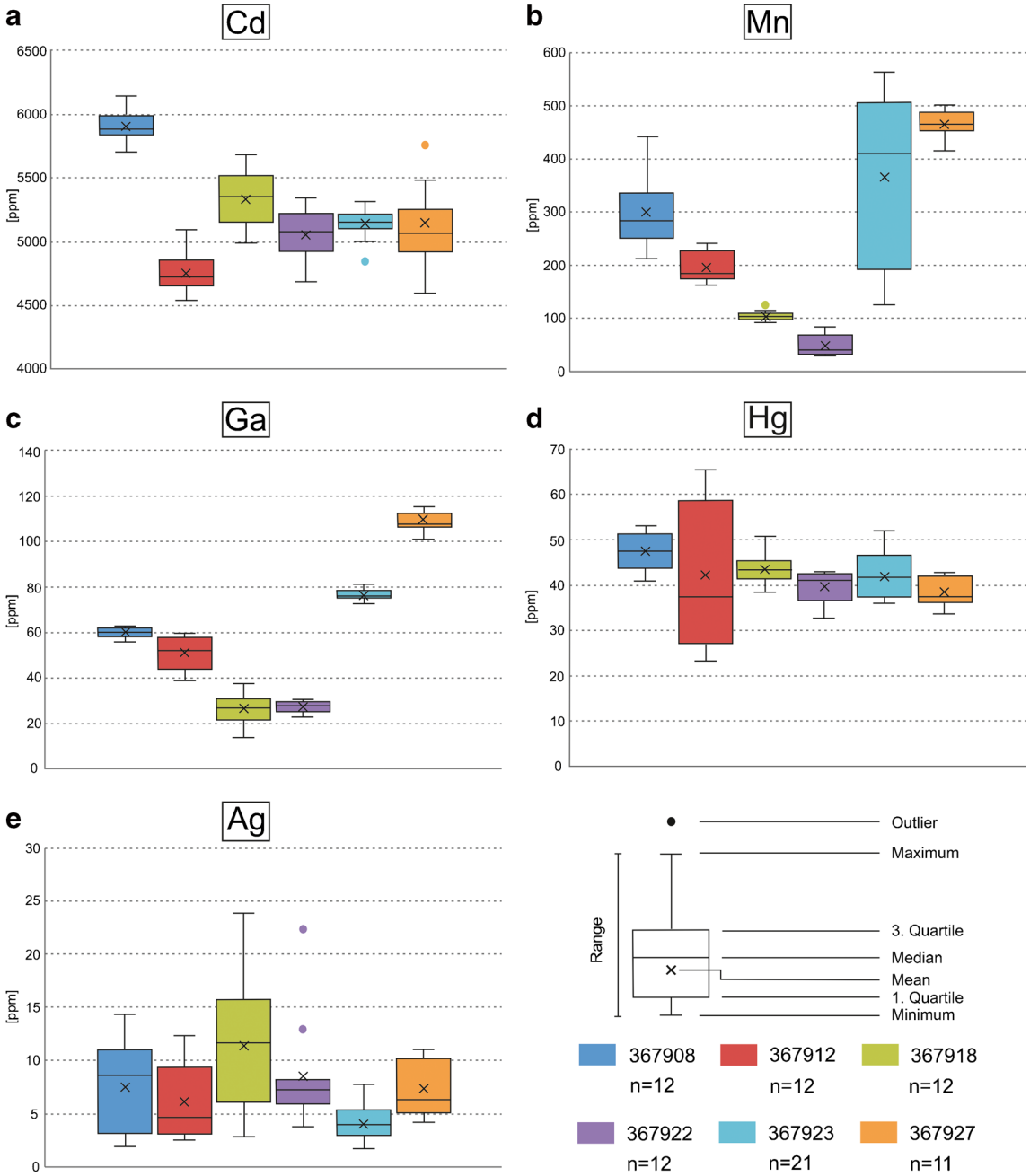

Fig. 7 Box- and whisker plots illustrating the trace element composition of sphalerite in samples 367908 (CZ), 367912 (V16Z), 367918 (BZ), 367922 (TZ), 367923 (DIZ), and 367927 (N1Z). **a** Cd in ppm; **b** Mn in ppm; **c** Ga in ppm; **d** Hg in ppm; **e** Ag in ppm. A spot analysis is considered to be an outlier if the concentration is 1.5 times higher or lower than the interquartile range. The abbreviations used for the different ore zones are given in ESM 1

This galena also has low Sn and Bi concentrations, but is enriched in Cd (282 ppm; Fig. 8e) and Mn (13 ppm). In general, however, the Cd concentration is relatively constant, with a mean concentration of 25 ppm. Thallium occurs in very low concentrations of up to 5 ppm. However, the mean concentration is near the detection limit of 1 ppm (ESM 4).

Chalcopyrite

Chalcopyrite was analyzed in five samples. Copper and Fe have a mean concentration of 34.37 and 29.81 wt.%, respectively (ESM 3). Trace element analyses could only be carried out in a sample from the banded ore, where the grains were

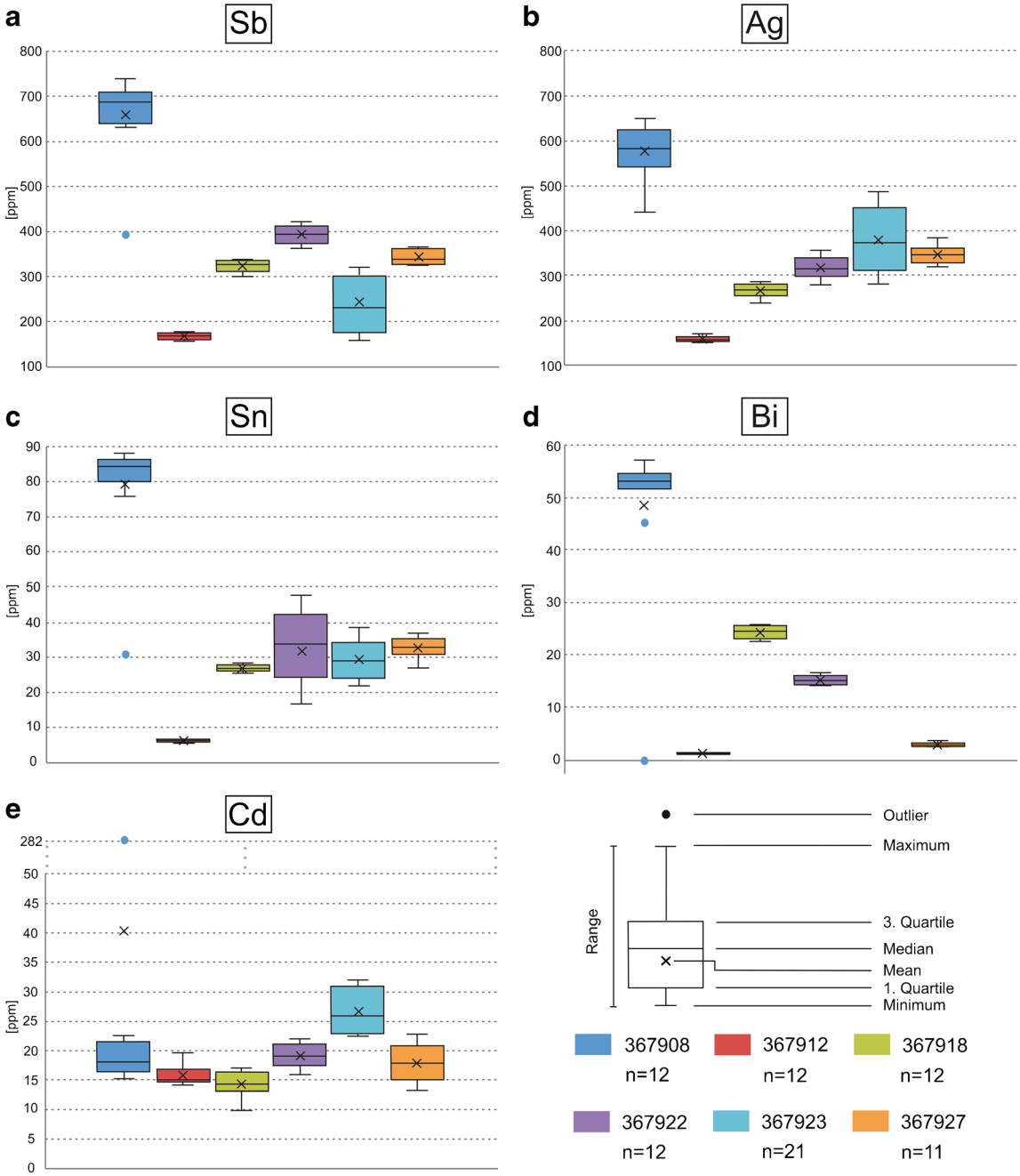

Fig. 8 Box- and whisker plots illustrating the trace element distribution in galena of samples 367908 (CZ), 367912 (V16Z), 367918 (BZ), 367922 (TZ), 367923 (DIZ), and 367927 (N1Z). **a** Sb in ppm; **b** Ag in ppm; **c** Sn in ppm; **d** Bi in ppm; **e** Cd in ppm. Note the outliers in element concentrations in sample 367908, which are due to pyrite inclusions. The abbreviations used for the different ore zones are given in ESM 1

large enough to be analyzed. Six spot analyses were conducted and the results indicate a broad range of trace element concentrations. In general, the grains contain high amounts of Zn, with a mean concentration of 2 wt.% (ESM 3). The Zn concentration shows a positive correlation with the Ge concentration, which reaches up to 1370 ppm (ESM 5). Tin and Ag are moderately enriched, with concentrations of up to 417 and 237 ppm, respectively. The concentrations of Ga and Sb are relatively low, with values of up to 61 and 42 ppm, respectively. The Cd and In concentrations are below 10 ppm (ESM 4). The Pb concentration reaches values of up to 4410 ppm, but the signal records fluctuations in the ablation

signal, which is likely due to a mixed analysis at the contact to galena. Lead concentrations in chalcopyrite are not considered in the further discussion.

Stannite group minerals

Briartite was identified as inclusion in sphalerite in the banded ore (ESM 3). Germanium has a mean concentration of 15.8 wt.%. Overall, the following formula is calculated: $Cu_{2.02}(Fe_{0.95}Zn_{0.12})(Ge_{0.86}Sn_{0.08})S_4$.

One sample from the porphyroclastic ore contains stannite as inclusion in sphalerite. Stannite measurements resulted in either too high or too low totals, which is most likely due to the small grain size and interaction with the surrounding sphalerite, as indicated by the high Zn content of analyses with totals above 100 wt.% (ESM 3). Nevertheless, the results show an enrichment in Ge in the range of several wt.%.

Tetrahedrite-freibergite

The major element composition of tetrahedrite-freibergite in the samples analyzed varies (ESM 3). The Ag content varies between 8.5 and 30.6 wt.%, whereas the Cu concentration ranges from 15.3 to 34 wt.%. Ag and Cu show a strong negative correlation ($R^2 = 0.996$).

Freibergite with a mean Ag concentration of 29.9 wt.% is present in one sample, while the other samples contain tetrahedrite with Ag concentrations at or below 15.8 wt.% (ESM 3). The lowest Ag concentration corresponds to the highest As (9.1 wt.%) and Cu (34 wt.%) concentrations and is recorded in tetrahedrite in contact with arsenopyrite (ESM 3; Fig. 5c).

Discussion

Paragenetic sequence

Based on the petrographic observations, the following paragenetic sequence is established for the porphyroclastic ore (Fig. 9). Type 1 pyrite and minor amounts of sphalerite, chalcopyrite, and galena that occur as inclusions in type 1 pyrite were the earliest sulfide minerals that precipitated. These inclusions, as well as type 1 pyrite, are locally associated with graphite. Apatite and zircon also occur as inclusion in type 1 pyrite and hence, are thought to be older than or of the same age as pyrite. Graphite is always accompanied by hydrothermal quartz and also surrounds quartz grains, which indicates a concurrent to slightly later precipitation. Type 1 pyrite is texturally early and often replaced by sphalerite, galena, quartz, or hydrothermal calcite (Fig. 4b). In addition, galena typically fills the interstitial space between sphalerite grains and replaces sphalerite along the rims. Therefore, the sphalerite replacing type 1 pyrite is interpreted to have precipitated prior to interstitial galena. Sphalerite replacing type 1 pyrite is accompanied by briartite, stannite, and rutile, while interstitial galena is associated with chalcopyrite, tetrahedrite-freibergite, and arsenopyrite (Fig. 9). In samples containing different pyrite generations (Fig. 4a, b), type 2 pyrite forms fine-grained euhedral grains or rims in association with sphalerite. However, it also contains sphalerite inclusions. Hydrothermal calcite precipitated in association with the late sphalerite and interstitial galena (Fig. 5f). Quartz is replaced by type 2 pyrite, galena, and calcite (Fig. 5f) and could therefore have precipitated prior to or contemporaneously with sphalerite.

Mineral textures

Pyrite annealing or "foam textures" are observed in three samples (Fig. 4a; ESM 1). These textures typically occur within areas of high pyrite content, where grain overgrowth and thermal annealing lead to an adjustment of grain boundary with ideal triple junctions (Craig and Vokes 1993). Pedersen (1981) also found these textures in pyrite from different ore tectonites in the Angel Zone.

Moreover, "Durchbewegung" textures and sphalerite twin lamellae as found here represent deformation microstructures (Gilligan and Marshall 1987) and are known from many metamorphosed sulfide deposits, such as those in the Norwegian Caledonides (Cook et al. 1993; Vokes and Craig 1993) and from the Cinco Villas Massif, Spain (Pesquera and Velasco 1993). Deformation of graphite is also common in metamorphic environments due to its low hardness and is also visible in the Black Angel deposit. However, the interstitial space- and fracture fillings of galena and chalcopyrite in more competent minerals may also be interpreted to indicate mobilization of sulfides by either partial melting or hydrothermal processes (Frost et al. 2002). The ore assemblages in Pb-Zn-Cu deposits start melting at about 700–730 °C at 2 kbar (Stevens et al. 2005). Additional elements such as Ag, Bi, and Sb can decrease the melting temperature (Tomkins et al. 2006). However, it is unlikely that these minor elements resulted in partial melting at greenschist facies conditions, which corresponds to temperatures below 500 °C (Frost et al. 2002). Hence, a combination of hydrothermal processes and deformation best explain the mineral textures at the Black Angel deposit.

Metamorphism and trace element distribution in the ore

The ore samples of the Black Angel deposit host several important minor and trace elements, including Cd, Ag, Ge, Sn as well as Ga and Sb.

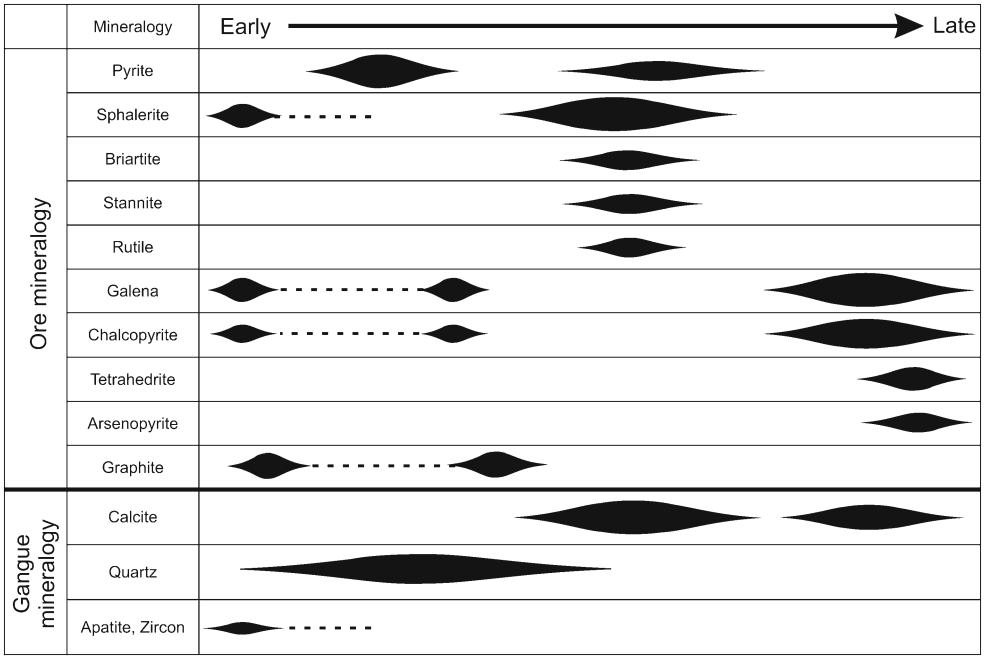

Fig. 9 Paragenetic sequence for the porphyroclastic ore of the Black Angel deposit. Early sulfides are type 1 pyrite and inclusions of sphalerite, galena, and chalcopyrite. Type 1 pyrite is replaced by sphalerite, accompanied by briartite, stannite, and rutile and type 2 pyrite. Galena, tetrahedrite-freibergite, and arsenopyrite fill the interstitial space between sphalerite grains. Quartz and graphite are associated with type 1 pyrite, while hydrothermal calcite occurs together with sphalerite and galena

Cadmium is primarily enriched in sphalerite with an average of 5220 ppm. It is, apart from its use in rechargeable nickel-cadmium batteries, a common environmental hazard and was a major problem during production at the Black Angel deposit (Thomassen 2006; Cook et al. 2009). Relatively constant concentrations of Cd as found here are commonly observed in sphalerite in metamorphosed deposits, which may be indicative of homogenization during metamorphism (Lockington et al. 2014).

Silver is mainly present in tetrahedrite-freibergite and galena. Despite the low abundance of tetrahedrite-freibergite in the samples analyzed, it is likely one of the main Ag-carriers with concentrations of up to 30.55 wt.%. Pedersen (1980) described larger occurrences of tetrahedrite, tennantite, and other Ag-bearing phases such as electrum and polybasite. Ag-rich tetrahedrite associated with galena and other sulfosalts has also been reported from metamorphosed, predominantly sediment-hosted deposits and syn-metamorphic Pb-Zn-Ag vein deposits (Riley 1974; Leach et al. 1988; Hoeller and Gandhi 1995; Cook 1996; Cook et al. 1998; Wu et al. 2018). However, the Ag concentration of galena in those deposits has not been analyzed by LA-ICP-MS. Galena from the Black Angel deposit contains Ag concentrations of up to 649 ppm. Likewise, Sb is primarily hosted in tetrahedrite-freibergite but also is an important trace element in galena with concentrations of up to 738 ppm. This reflects the coupled substitution $Ag^{+} + (Sb, Bi)^{3+} \leftrightarrow 2\ Pb^{2+}$ needed to incorporate significant quantities of Ag into the crystal structure of galena (Chutas et al. 2008).

Germanium is generally depleted in sphalerite and was found primarily in briartite and stannite. Briartite is only known from a few localities worldwide. It was first discovered in the Kipushi Mine in the Democratic Republic of the Congo (Francotte et al. 1965) and is now known from other mainly carbonate-hosted base metal deposits such as Kabwe in Zambia and Tsumeb in Namibia, many of which show polymetallic styles of mineralization and are often ascribed to as Kipushi-type (KPT) deposits (Trueman 1998; Höll et al. 2007). In these deposits, briartite occurs primarily as microscopic inclusions in sphalerite, accompanied by other Ge-minerals such as renierite and germanite (Höll et al. 2007). Those minerals have so far not been identified in the Black Angel deposit. Notably, the Kabwe deposit also contains Ge-rich chalcopyrite that is similar in composition to that of the Black Angel deposit, and the Kabwe deposit also experienced metamorphism in the greenschist facies (Kamona and Friedrich 2007). A close relationship between Ge and Sn due to their chemical similarity is seen by the substitution of Ge and Sn in briartite and stannite. Both metals are also abundant in chalcopyrite, with a mean concentration of 326 ppm Ge and 324 ppm Sn (ESM 6). Syn-metamorphic vein deposits from the Barrigão deposit in the Iberian Pyrite Belt, Portugal, contain Sn-enriched chalcopyrite with up to 1.88 wt.% Sn, which correlates with high Ge concentrations of up to 0.64 wt.% and the occurrence of Sn-Ge-bearing phases, possibly stannite or briartite (Reiser et al. 2011). These data show that both metals can be mobilized during metamorphism. In addition, George et al. (2015, 2016) observed an enrichment of Sn in chalcopyrite in metamorphosed deposits followed by galena, comparable to the Sn concentration in the Black Angel deposit.

Mobilization and enrichment of trace elements in chalcopyrite and galena during metamorphism have also been reported for Ga and In (George et al. 2016). However, Ga

at the Black Angel deposit is primarily incorporated in sphalerite, while In concentrations are generally low and show no significant difference between sphalerite, chalcopyrite, and galena (ESM 6). Thus, mobilization of Ga and In during metamorphism at the Black Angel deposit is unlikely.

Formation of Ge-Sn-rich phases and sulfidation state of the hydrothermal fluid

Briartite in the Black Angel deposit was only found in the banded ore, which was interpreted as the primary ore that was deformed during regional metamorphism (Pedersen 1980). It is thus possible that Ge and Sn were originally incorporated in sphalerite and that the formation of Ge-Sn-rich phases is a result of recrystallization of sphalerite during a metamorphic overprint. However, the deformation textures in the banded ore, such as elongate grain shapes of pyrite or twin lamellae in sphalerite (Pedersen 1980, 1981), are consistent with a syn-tectonic style of mineralization, and the banding in the banded ore is axial planar to D_1BA (Fig. 3). The banding is thus most likely not a primary feature but a product of metamorphism and deformation, as it is commonly observed in, e.g., metamorphosed volcanic-hosted massive sulfide (VHMS) deposits (Galley et al. 2007). We therefore interpret the Ge-Sn phases as precipitates from a hydrothermal fluid. Studies on Ge geochemistry show that an intermediate to high sulfidation state in hydrothermal fluids leads to the preferred precipitation of Ge-sulfides or incorporation of Ge in Sn- and Cu-sulfide minerals such as stannite or chalcopyrite, rather than substituting Zn in sphalerite, which is preferred at low sulfidation state (Bernstein 1985; Paar and Putz 2005; Höll et al. 2007). An example for the formation of Ge-sulfides at high sulfidation state is high sulfidation epithermal deposits, where Ge is mainly incorporated in argyrodite and enargite (Sahlström et al. 2017) or germanite, renierite, germanocolusite, and briartite (Bodganov et al. 2004). An elevated sulfidation state during mineralization at the Black Angel deposit is also consistent with the presence of enargite (Pedersen 1980). However, the generally low to moderate Fe contents of sphalerite (2–9 mol% FeS; ESM 3) as well as the presence of chalcopyrite and arsenopyrite in the ore indicate a dominantly intermediate sulfidation state throughout the development of this hydrothermal system (Fig. 9; Einaudi et al. 2003; Petersen et al. 2014). This is consistent with the fact that at temperatures above 300 °C, enargite coexists with chalcopyrite at intermediate sulfidation states (Einaudi et al. 2003; Petersen et al. 2014).

Implications on ore deposition

Two deposit types, SHMS and MVT, have been suggested to explain the hydrothermal Zn-Pb-Ag style of mineralization in the Black Angel deposit (Leach et al. 2005; Thomassen 2006). Several observations and data presented here, however, contradict a syngenetic hydrothermal origin of the ore at Black Angel: (1) the ore is often hosted in breccia; (2) sulfides are elongated in the banded ore and the banding is axial planar to fold structures; and (3) petrographic and structural observations indicate a hydrothermal style of mineralization that was coeval with deformation and metamorphism. Furthermore, unpublished fluid inclusion data yields estimated temperatures of 400–450 °C for the hydrothermal fluids (Konnerup-Madsen; personal communication 2016), which is unusually high for SHMS deposits (Emsbo 2009).

The carbonate-dominated host rocks, locally breccia-like ore textures and the setting of the deposit in a carbonate platform sequence, are typical of MVT deposits (Corbella et al. 2004; Leach et al. 2010a). Rosa et al. (2017) proposed a MVT style of mineralization based on the presence of anhydrite in the Mârmorilik Formation. Evaporites are a possible source of sulfur, and evaporite dissolution is common in MVT deposits, as indicated by highly saline brines (Leach et al. 2010a). The samples from this study include massive anhydrite, and anhydrite-bearing calcitic marble was also described by Pedersen (1980). However, anhydrite in the Mârmorilik Formation or at Black Angel Mountain is unlikely to reflect the source of sulfur due to the short distance to the ore deposit, and other formations of the Karrat Group do not contain evaporites. An alternative source of sulfur would be sulfate-enriched connate seawater or basinal brines. Nevertheless, a generally epigenetic style of mineralization at Black Angel is indicated by the Pb-Zn showings in the South Lakes area (Fig. 10). Here, the massive sulfides surround angular and folded marble fragments, which implies an ore deposition synchronous with or postdating regional deformation.

Some of our observations in the Black Angel deposit are, however, atypical of MVT deposits. MVT deposits are generally unrelated to metamorphic rocks or processes (Leach et al. 2010a). The Ge concentration in sphalerite from Black Angel is low (< 100 ppm) compared to MVT deposits, and the main carrier of Ge at Black Angel is briartite. This is more similar to KPT deposits, which generally have low Ge concentration in sphalerite (Höll et al. 2007; Bellisont et al. 2015), while Ge-phases and sulfosalts are distinctive (Melcher 2003).

An origin as a KPT deposit is thus considered to be a possible model for the Black Angel deposit. KPT deposits are similar to MVT deposits in that they are epigenetic and evaporites or seawater appear to be the main source of sulfur

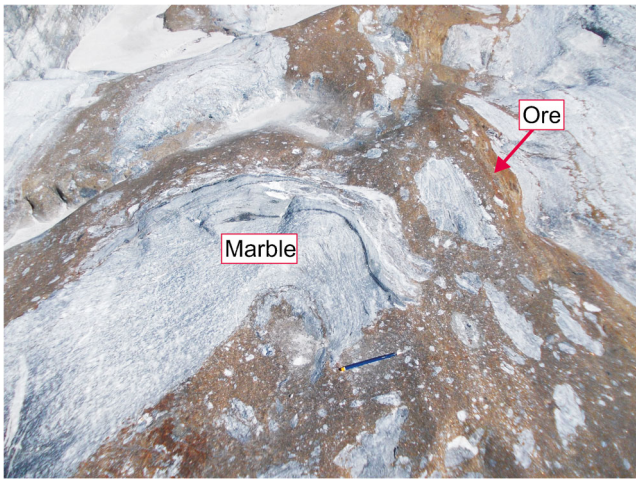

Fig. 10 Angular and folded marble fragments surrounded by sulfides in the South Lakes area. Pencil for scale

(Chetty and Frimmel 2000). However, they are characterized by variable amounts of additional metals such as Ge, Ga, In, Sn, Sb, V, W, and Au in the mainly Pb-Zn-Cu ores (Melcher 2003; Höll et al. 2007). The setting of KPT deposits is described as intracratonic platform and rifted continental margin sedimentary successions, dominated by dolostone or limestone (Trueman 1998). The orebodies in KPT deposits are mainly massive, pipe-like to tabular-shaped, and irregular and locally related to breccias, similar to those in the Black Angel deposit (Trueman 1998; Höll et al. 2007; Kampunzu et al. 2009). The mineralogy of the orebodies at the Black Angel deposit is similar to those from the Kabwe deposit, the latter being dominated by massive sphalerite, galena, and pyrite, with minor amounts of chalcopyrite, briartite, germanite, and renierite, which occur primarily as microscopic inclusions in sphalerite (Höll et al. 2007; Kamona and Friedrich 2007). Germanite and renierite have so far not been identified in the Black Angel deposit. Another similarity is that much of the ore appears to have formed syn-tectonically and the wall rocks experienced greenschist facies metamorphism (Pedersen 1980; Kamona et al. 1999; Kamona and Friedrich 2007).

The estimated temperatures of mineralization for KPT deposits are typically higher compared to MVT deposits. The Tsumeb deposit formed at a temperature of 370–405 °C (Chetty and Frimmel 2000). This temperature range is similar to the 400–450 °C estimated for the hydrothermal mineralization in the Black Angel deposit (Konnerup-Madsen; personal communication 2016), but distinctly higher than the temperatures typically recorded from MVT deposits (70–250 °C; Leach et al. 2010a).

In a recent study, Frenzel et al. (2016) showed that the elements Fe, Mn, Ga, Ge, and In show statistically significant differences in mean concentration in sphalerite from different deposit types, including MVT, SHMS, VHMS, vein type deposits, and high temperature hydrothermal deposits (HTHR). The trace element content of sphalerite varies with temperature and can be used as a geothermometer. However, the application of the "Ga-Ge-In-Mn-Fe in sphalerite" (GGIMFis) thermometer to our samples was not possible because the trace element systematics on which the thermometer is based on do not exist in sphalerite of the Black Angel deposit. Our data suggest that the GGIMFis thermometer cannot be applied to deposits containing Ge-bearing sulfide inclusions in sphalerite, consistent with a generally low Ge concentration in sphalerite from KPT deposits (Höll et al. 2007; Bellisont et al. 2015).

Despite the distinguishing features of MVT and KPT deposits, it should be noted that many of the above mentioned characteristics of the different deposit types are similar and there are transitions between them. However, the timing of mineralization yields an important difference. MVT deposits are epigenetic and primarily related to the evolution of orogenic belts and compressional deformation after basin inversion (Leach et al. 2010b). The Maarmorilik area similarly experienced an extensional stage followed by a compressional deformation stage. The axial planar banding in the banded ore, local presence of breccia textures, and the massive ore at South Lakes (Figs. 3 and 10) show that the sulfides were deposited during or after regional deformation, indicating most likely a KPT style of mineralization.

Conclusion

1. Minor and trace element analysis of sulfide minerals at Black Angel reveals that Ge is mainly incorporated in briartite, stannite, and chalcopyrite rather than being enriched in sphalerite. The enrichment of Ge and Sn in chalcopyrite and Cu-Fe-Sn-Ge sulfides implies a mobilization of these elements during metamorphism and an intermediate sulfidation state of the ore fluid.
2. Silver is primarily enriched in galena and tetrahedrite-freibergite, the latter of which contains up to 30.5 wt.% Ag. Galena, which commonly encloses tetrahedrite-freibergite, contains moderate amounts of Ag (up to 649 ppm).
3. Similarities of the Black Angel deposit to MVT deposits include the carbonate host-rock and hydrothermal breccias, but the ore is syn-tectonic and syn-metamorphic. Banding parallel to axial planes in the banded ore is reinterpreted to have formed as a result of deformation rather than indicating a syngenetic deposition typical of SHMS deposits. A deposition style similar to KPT

deposits is thus most likely as these are the main ore deposits from which briartite has been documented, the mineralization is epigenetic and some KPT deposits are syn-tectonic and syn-metamorphic.

4. Mineralogical and mineral-chemical analysis identified a hitherto unknown potential of Ge at the Black Angel deposit.

Acknowledgments This study presents the results of a M.Sc. project carried out by Stefan Horn at the Institute of Applied Mineralogy and Economic Geology at RWTH Aachen University. The samples used in this study were provided by the Geological Survey of Denmark and Greenland (GEUS). We gratefully acknowledge the support of the GEUS team, especially Bjørn Thomassen for preparing the samples and providing additional information and Diogo Rosa for fruitful discussions on briartite and the origin of the Black Angel deposit. We would like to thank Associate Editor Thomas Monecke, Cora Wohlgemuth-Ueberwasser, and an anonymous reviewer for their valuable and constructive comments, which considerably improved the manuscript. Bernd Lehmann is thanked for editorial handling.

References

Barton PB, Bethke PM (1987) Chalcopyrite disease in sphalerite; pathology and epidemiology. Am Mineral 72:451–467

Bellisont R, Boiron M, Luais B, Muchez P, de Oliveira D, Munoz M (2015) Germanium distribution and isotopic study in sulphides from MVT-related and VMS-remobilised ore deposits. In: André-Mayer AS, Cathelineau M, Muchez P, Pirard E, Sindern S (eds) Mineral resources in a sustainable world. Proceedings of the 13th Biennial SGA Meeting, Nancy, France, pp 683–686

Bente K, Doering T (1993) Solid-state diffusion in sphalerites: an experimental verification of the "chalcopyrite disease". Eur J Mineral 5: 465–478

Bente K, Doering T (1995) Experimental studies on the solid state diffusion of cu + in in ZnS and on “disease” DIS (diffusion induced segregations), in sphalerite and their geological applications. Mineral Petrol 53:285–305. https://doi.org/10.1007/BF01160153

Bernstein LR (1985) Germanium geochemistry and mineralogy. Geochim Cosmochim Acta 49:2409–2422. https://doi.org/10.1016/0016-7037(85)90241-8

Bodganov K, Tsonev D, Popov K (2004) Mineral assemblages and genesis of the cu-au epithermal deposits in the southern part of the Panaguyrishte ore district, Bulgaria. Bull Geol Soc Greece 36: 406–415

Chetty D, Frimmel HE (2000) The role of evaporites in the genesis of base metal sulphide mineralisation in the northern platform of the Pan-African Damara Belt, Namibia: geochemical and fluid inclusion evidence from carbonate wall rock alteration. Mineral Deposita 35: 364–376. https://doi.org/10.1007/s001260050247

Chutas NI, Kress VC, Ghiorso MS, Sack RO (2008) A solution model for high-temperature PbS-$AgSbS_2$-$AgBiS_2$ galena. Am Mineral 93: 1630–1640. https://doi.org/10.2138/am.2008.2695

Connelly JN, Thrane K, Krawiec AW, Garde AA (2006) Linking the Palaeoproterozoic Nagssugtoqidian and Rinkian orogens through the Disko Bugt region of West Greenland. J Geol Soc Lond 163: 319–335. https://doi.org/10.1144/0016-764904-115

Cook NJ (1996) Mineralogy of the sulphide deposits at Sulitjelma, northern Norway. Ore Geol Rev 11:303–338. https://doi.org/10.1016/S0169-1368(96)00009-1

Cook NJ, Halls C, Boyle AP (1993) Deformation and metamorphism of massive sulphides at Sulitjelma, Norway. Mineral Mag 57:67–81. https://doi.org/10.1180/minmag.1993.057.386.07

Cook NJ, Spry PG, Vokes FM (1998) Mineralogy and textural relationships among sulphosalts and related minerals in the Bleikvassli Zn-Pb-(cu) deposit, Nordland, Norway. Mineral Deposita 34:35–56. https://doi.org/10.1007/s001260050184

Cook NJ, Ciobanu CL, Pring A, Skinner W, Shimizu M, Danyushevsky L, Saini-Eidukat B, Melcher F (2009) Trace and minor elements in sphalerite: a LA-ICPMS study. Geochim Cosmochim Acta 73: 4761–4791. https://doi.org/10.1016/j.gca.2009.05.045

Corbella M, Ayora C, Cardellach E (2004) Hydrothermal mixing, carbonate dissolution and sulfide precipitation in Mississippi Valley-type deposits. Mineral Deposita 39:344–357. https://doi.org/10.1007/s00126-004-0412-5

Craig JR, Vokes FM (1993) The metamorphism of pyrite and pyritic ores: an overview. Mineral Mag 57:3–18. https://doi.org/10.1180/minmag.1993.057.386.02

Einaudi MT, Hedenquist JW, Inan EE (2003) Sulfidation state of fluids in active and extinct hydrothermal systems: transitions from porphyry to epithermal environments. Soc Econ Geol Spec P 10:285–314

Emsbo P (2009) Geologic criteria for the assessment of sedimentary exhalative (SEDEX) Zn-Pb-ag deposits. U.S. Geological Survey. https://pubs.usgs.gov/of/2009/1209/pdf/OF09-1209.pdf. Accessed 7 May 2018

Francotte J, Moreau J, Ottenburgs R, Levy C (1965) La briartite, Cu_2(Fe, Zn)GeS_4, une nouvelle espèce minérale. Bull Soc Fr Mineral Cristallogr 88:432–437

Frenzel M, Hirsch T, Gutzmer J (2016) Gallium, germanium, indium, and other trace and minor elements in sphalerite as a function of deposit type — a meta-analysis. Ore Geol Rev 76:52–78. https://doi.org/10.1016/j.oregeorev.2015.12.017

Frost BR, Mavrogenes JA, Tomkins AG (2002) Partial melting of sulfide ore deposits during medium- and high-grade metamorphism. Can Mineral 40:1–18. https://doi.org/10.2113/gscanmin.40.1.1

Galley AG, Hannington MD, Jonasson IR (2007) Volcanogenic massive sulphide deposits. In: Goodfellow WD (ed) Mineral deposits of Canada: A synthesis of major deposit-types, district metallogeny, the evolution of geological provinces, and exploration methods: Geological Association of Canada, Mineral Deposits Division Special Publication 5, St. Johns, pp 141–161

Garde AA (1978) The lower Proterozoic Marmorilik formation, east of Mârmorilik, West Greenland. Meddr Gronland 200, 71p

George L, Cook NJ, Ciobanu CL, Wade BP (2015) Trace and minor elements in galena: a reconnaissance LA-ICP-MS study. Am Mineral 100:548–569. https://doi.org/10.2138/am-2015-4862

George LL, Cook NJ, Ciobanu CL (2016) Partitioning of trace elements in co-crystallized sphalerite–galena–chalcopyrite hydrothermal ores. Ore Geol Rev 77:97–116. https://doi.org/10.1016/j.oregeorev.2016.02.009

Gilligan LB, Marshall B (1987) Textural evidence for remobilization in metamorphic environments. Ore Geol Rev 2:205–229. https://doi.org/10.1016/0169-1368(87)90029-1

Greenex A/S (1990) Mine maps of Maarmorilik. Modified by geological survey of Denmark and Greenland (GEUS)

Grocott J, McCaffrey KJW (2017) Basin evolution and destruction in an early Proterozoic continental margin: the Rinkian fold and thrust belt of central West Greenland. J Geol Soc Lond 174:453–467. https://doi.org/10.1144/jgs2016-109

Grocott J, Pulvertaft T (1990) The early Proterozoic Rinkian belt of central West Greenland. In: Lewry JF, Stauffer MR (eds) The early Proterozoic trans-Hudson Orogen of North America, Geological Association of Canada Special Paper 37, pp 443–463

Hattendorf B (2000) Worksheet for LA-ICPMS analysis: Microsoft excel. In: Laboratory of inorganic chemistry. ETH Zürich, Switzerland

Henderson G, Pulvertaft T (1967) The stratigraphy and structure of the Precambrian rocks of the Umanak area, West Greenland. Medd Dansk Geol Føren 17:1–20

Hoeller W, Gandhi SM (1995) Silver-bearing sulfosalts from the metamorphosed Rampura Agucha Zn-Pb-(ag) deposit, Rajasthan, India. Can Mineral 33:1047–1057

Höll R, Kling M, Schroll E (2007) Metallogenesis of germanium—a review. Ore Geol Rev 30:145–180. https://doi.org/10.1016/j.oregeorev.2005.07.034

Kamona AF, Friedrich GH (2007) Geology, mineralogy and stable isotope geochemistry of the Kabwe carbonate-hosted Pb-Zn deposit, Central Zambia. Ore Geol Rev 30:217–243. https://doi.org/10.1016/j.oregeorev.2006.02.003

Kamona AF, Lévêque J, Friedrich G, Haack U (1999) Lead isotopes of the carbonate-hosted Kabwe, Tsumeb, and Kipushi Pb-Zn-cu sulphide deposits in relation to Pan African orogenesis in the Damaran-Lufilian Fold Belt of Central Africa. Mineral Deposita 34:273–283. https://doi.org/10.1007/s001260050203

Kampunzu AB, Cailteux J, Kamona AF, Intiomale MM, Melcher F (2009) Sediment-hosted Zn–Pb–cu deposits in the central African Copperbelt. Ore Geol Rev 35:263–297. https://doi.org/10.1016/j.oregeorev.2009.02.003

Kolb J, Keiding JK, Steenfelt A, Secher K, Keulen N, Rosa D, Stensgaard BM (2016) Metallogeny of Greenland. Ore Geol Rev 78:493–555. https://doi.org/10.1016/j.oregeorev.2016.03.006

Leach DL, Landis GP, Hofstra AH (1988) Metamorphic origin of the Coeur d'Alene base- and precious-metal veins in the belt basin, Idaho and Montana. Geology 16:122–125

Leach DL, Sangster DF, Kelley KD, Ross RL, Garven G, Allen CR (2005) Sediment-hosted Pb-Zn deposits: a global perspective. Econ Geol 100:561–608

Leach DL, Taylor RD, Fey DL, Diehl SF, Saltus RW (2010a) A deposit model for Mississippi Valley-type lead-zinc ores: Chapter A in Mineral deposit models for resource assessment. Scientific Investigations Report (2010–5070-A), 43p

Leach DL, Bradley DC, Huston D, Pisarevsky SA, Taylor RD, Gardoll SJ (2010b) Sediment-hosted lead-zinc deposits in earth history. Econ Geol 105:593–625. https://doi.org/10.2113/gsecongeo.105.3.593

Lockington JA, Cook NJ, Ciobanu CL (2014) Trace and minor elements in sphalerite from metamorphosed sulphide deposits. Mineral Petrol 108:873–890. https://doi.org/10.1007/s00710-014-0346-2

Melcher F (2003) The Otavi Mountain land in Namibia: Tsumeb, germanium and snowball earth. Mitt Österr Miner Ges 148:413–435

Paar WH, Putz H (2005) Germanium associated with epithermal mineralization: examples from Bolivia and Argentina. In: Mao J, Bierlein FP (eds) Mineral deposit research: meeting the global challenge, v 3. Beijing, pp 48–51

Pedersen FD (1980) Remobilization of the massive sulfide ore of the black angel mine, central West Greenland. Econ Geol 75:1022–1041. https://doi.org/10.2113/gsecongeo.75.7.1022

Pedersen FD (1981) Polyphase deformation of the massive sulphide ore of the black angel mine, central West Greenland. Mineral Deposita 16:157–176. https://doi.org/10.1007/BF00206461

Pesquera A, Velasco F (1993) Ore metamorphism in sulfide mineralizations from the Cinco villas massif (western Pyrenees, Spain). Econ Geol 88:266–282. https://doi.org/10.2113/gsecongeo.88.2.266

Petersen S, Monecke T, Westhues A, Hannington MD, Gemmell JB, Sharpe R, Peters M, Strauss H, Lackschewitz K, Augustin N, Gibson H, Kleeberg R (2014) Drilling shallow-water massive sulfides at the Palinuro volcanic complex, Aeolian Island arc, Italy. Econ Geol 109:2129–2158. https://doi.org/10.2113/econgeo.109.8.2129

Reiser FK, Rosa DR, Pinto ÁM, Carvalho JR, Matos JX, Guimarães FM, Alves LC, de ODP (2011) Mineralogy and geochemistry of tin- and germanium-bearing copper ore, Barrigão re-mobilized vein deposit, Iberian Pyrite Belt, Portugal. Int Geol Rev 53:1212–1238. https://doi.org/10.1080/00206811003683168

Riley JF (1974) The tetrahedrite-freibergite series, with reference to the Mount Isa Pb-Zn-ag orebody. Mineral Deposita 9:117–124. https://doi.org/10.1007/BF00207969

Rosa D, Guarnieri P, Hollis J, Kolb J, Partin C, Petersen J, Sørensen EV, Thomassen B, Thomsen L, Thrane K (2016) Architecture and mineral potential of the Paleoproterozoic Karrat group, West Greenland: results of the 2015 season. Geological survey of Denmark and Greenland, Report, 2017/5, 112 p

Rosa D, Dewolfe M, Guarnieri P, Kolb J, Laflamme C, Partin C, Salehi S, Sørensen EV, Thaarup S, Thrane K, Zimmermann R (2017) Architecture and mineral potential of the Paleoproterozoic Karrat group, West Greenland: results of the 2016 season. Geological survey of Denmark and Greenland, Report, 2016/12, 98 p

Sahlström F, Arribas A, Dirks P, Corral I, Chang Z (2017) Mineralogical distribution of germanium, gallium and indium at the Mt Carlton high-sulfidation epithermal deposit, NE Australia, and comparison with similar deposits worldwide. Mineral Basel 7:213. https://doi.org/10.3390/min7110213

Sanborn-Barrie M, Thrane K, Wodicka N, Rayner N (2017) The Laurentia–West Greenland connection at 1.9 Ga: new insights from the Rinkian fold belt. Gondwana Res 51:289–309. https://doi.org/10.1016/j.gr.2017.07.002

Stevens G, Prinz S, Rozendaal A (2005) Partial melting of the assemblage sphalerite + galena + pyrrothite + chalcopyrite + sulfur: implications for high-grade metamorphosed massive sulfide deposits. Econ Geol 100:781–786. https://doi.org/10.2113/gsecongeo.100.4.781

St-Onge MR, van Gool JAM, Garde AA, Scott DJ (2009) Correlation of Archaean and Palaeoproterozoic units between northeastern Canada and western Greenland: constraining the pre-collisional upper plate accretionary history of the trans-Hudson orogen. In: Cawood PA, Kröner A (eds.) Earth Accretionary Systems in Space and Time, The Geological Society, London 318. pp 193–235. https://doi.org/10.1144/SP318.7

Sugaki A, Kitakaze A, Kojima S (1987) Bulk compositions of intimate intergrowths of chalcopyrite and sphalerite and their genetic implications. Mineral Deposita 22:26–32. https://doi.org/10.1007/BF00204240

Taylor PN, Kalsbeek F (1990) Dating the metamorphism of Precambrian marbles: examples from Proterozoic mobile belts in Greenland. Chem Geol 86:21–28. https://doi.org/10.1016/0168-9622(90)90003-U

Thomassen B (2006) The black angel lead-zinc mine at Maarmorilik in West Greenland. Geology and Ore (Geological Survey of Denmark and Greenland) 2, 12p

Thrane K, Baker J, Connelly J, Nutman A (2005) Age, petrogenesis and metamorphism of the syn-collisional Prøven igneous complex, West Greenland. Contrib Mineral Petrol 149:541–555. https://doi.org/10.1007/s00410-005-0660-0

Tomkins AG, Pattison DRM, Frost BR (2006) On the initiation of metamorphic sulfide anatexis. J Petrol 48:511–535. https://doi.org/10.1093/petrology/egl070

Trueman EAG (1998) Carbonate hosted Cu±Pb±Zn in geological fieldwork 1997. British Columbia Ministry of Employment and Investment (Paper 1998–1), pp 24B-1–24B-4

van Gool JA, Connelly JN, Marker M, Mengel FC (2002) The Nagssugtoqidian Orogen of West Greenland: tectonic evolution and regional correlations from a West Greenland perspective. Can J Earth Sci 39:665–686. https://doi.org/10.1139/e02-027

Vokes FM (1969) A review of the metamorphism of sulphide deposits. Earth Sci Rev 5:99–143. https://doi.org/10.1016/0012-8252(69)90080-4

Vokes FM, Craig JR (1993) Post-recrystallisation mobilisation phenomena in metamorphosed stratabound sulphide ores. Mineral Mag 57:19–28

Wilson SA, Ridley WI, Koenig AE (2002) Development of sulfide calibration standards for the laser ablation inductively-coupled plasma mass spectrometry technique. J Anal At Spectrom 17:406–409. https://doi.org/10.1039/B108787H

Wu S, Mao J, Yuan S, Dai P, Wang X (2018) Mineralogy, fluid inclusion petrography, and stable isotope geochemistry of Pb–Zn–ag veins at the Shizhuyuan deposit, Hunan Province, southeastern China. Mineral Deposita 53:89–103. https://doi.org/10.1007/s00126-017-0725-9